Efficient coupling between dielectric and hybrid plasmonic waveguides by multimode interference power splitter

2011 J. Opt. 13 075002

(http://iopscience.iop.org/2040-8986/13/7/075002)

IOP Publishing Journal of Optics

J. Opt. **13** (2011) 075002 (7pp) doi:10.1088/2040-8978/13/7/075002

Efficient coupling between dielectric and hybrid plasmonic waveguides by multimode interference power splitter

Yi Song, Jing Wang, Min Yan and Min Qiu

Laboratory of Photonics and Microwave Engineering, School of Information and Communication Technology, Royal Institute of Technology, Electrum 229, S-164 40 Kista, Sweden

E-mail: min@kth.se (M Qiu)

Received 1 February 2011, accepted for publication 7 April 2011
Published 28 April 2011
Online at stacks.iop.org/JOpt/13/075002

Abstract
Multimode interference power splitters based on hybrid plasmonic waveguides are investigated

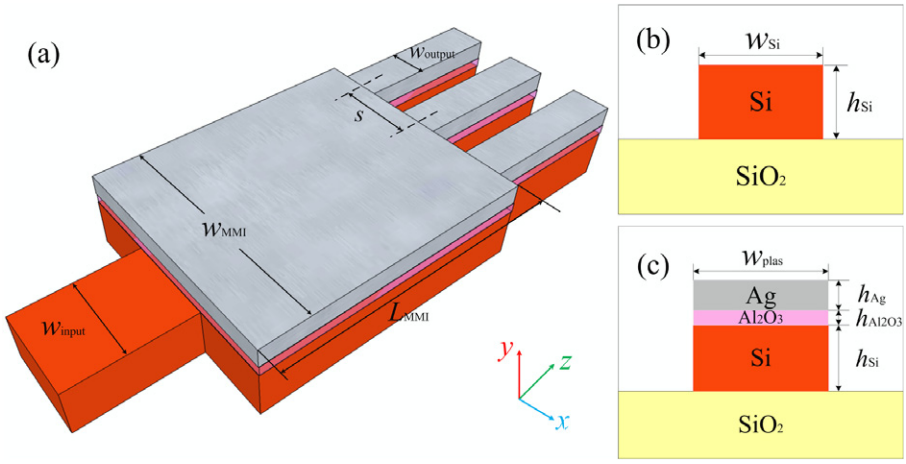

Figure 1. (a) Schematic diagram of the 1 × 3 SOI-HP MMI power splitter. The HP waveguide-based MMI regime has a width w_{MMI} and length L_{MMI}. The input SOI waveguide has a width w_{input}. The output HP waveguides have a width w_{output} and the separation between them is s. (b) The cross section of an SOI waveguide with the width w_{Si} and height h_{Si}. (c) The cross section of an HP waveguide composed by depositing an alumina layer (h_{Al2O3}) and then a silver layer (h_{Ag}) on top of an SOI waveguide with a height h_{Si} and width w_{plas}.

the total coupling efficiency as high as 76.1% and 78.3% for the designed 1 × 3 and 1 × 2 SOI-HP MMI power splitters, respectively.

2. Self-imaging principle

MMI power splitters rely on the self-imaging principle, by which the input field profile is reproduced as multiple-fold images at certain propagation distances [19]. At the entrance of the MMI regime, the input field profile $\Phi(0)$ will be decomposed into all guided modes $\varphi_v(0)$ supported by the multimode waveguide:

$$\Phi(0) = \sum_{v=0}^{m-1} a_v \varphi(0) \tag{1}$$

where the coefficient a_v is the modal amplitude and v is the mode number. At a distance $z = L$, the profile has the form [19]

$$\Phi(L) \approx \sum_{v=0}^{m-1} a_v \varphi(0) \exp\left(\mathrm{i}\frac{v(v+2)\pi}{3L_\pi}L\right) \tag{2}$$

where $L_\pi = \pi/(\beta_0 - \beta_1)$ is the beating length of the two lowest-order modes, and $\beta_0 = n_0 k_0$ and $\beta_1 = n_1 k_0$ are propagation constants of the two modes. Then $\Phi(L)$ will be a single image of $\Phi(0)$ at a distance $L = p(3L_\pi)$ ($p = 1, 2, 3, \ldots$), where $\exp(\mathrm{i}\frac{v(v+2)\pi}{3L_\pi}L) = 1$ or $(-1)^v$, and N-fold images will occur at distances of $L = p(3L_\pi)/N$ [19]. If the input waveguide is connected to the center of the multimode waveguide, only even modes ($v = 0, 2, 4, \ldots$) can be excited and the corresponding N-fold images are expected to be formed at much shorter distances [19]:

$$L = \frac{p}{N}\left(\frac{3L_\pi}{4}\right) = \frac{p}{N}\frac{3\lambda}{8}\frac{1}{(n_0 - n_1)}. \tag{3}$$

Such a reduction in the length of the MMI regime directly leads to a smaller loss owing to ohmic absorption in our proposed plasmonic waveguide system. Due to this factor, all MMI structures designed in this study use such a central in-coupling configuration.

For an MMI, imaging resolution is an important parameter which refers to the accuracy of the reproduction of the input field [19]. To obtain a 1 × N splitter with high imaging resolution, the multimode waveguide is required to support at least $N + 1$ modes [21].

3. SOI-HP MMI power splitters

A schematic diagram of the designed SOI-HP MMI power splitter is depicted in figure 1(a). The input waveguide is a standard SOI waveguide composed of a silicon waveguide ($h_{\mathrm{Si}} = 250$ nm, $w_{\mathrm{Si}} = 450$ nm) on the 3 μm thick silica substrate (figure 1(b)) for which only a fundamental transverse electric (TE) mode and a fundamental transverse magnetic (TM) mode are supported at the wavelength of 1550 nm. The MMI regime and the output access waveguides are based on an HP waveguide system which can be fabricated by depositing an alumina layer (of thickness $h_{\mathrm{Al2O3}} = 50$ nm in the proposed structure) and then a silver layer (of thickness $h_{\mathrm{Ag}} = 100$ nm) on top of SOI waveguides (figure 1(c)). Here, a finite-element method (FEM)-based commercial software COMSOL Multiphysics is used to simulate the complex effective indices, propagation lengths and transverse field profiles for the HP waveguide, at various widths, that constitutes our proposed MMI power splitter. Since the intended operating wavelength is around the telecommunication wavelength, the parameters of the materials are set to be $n_{\mathrm{Si}} = 3.45$, $n_{\mathrm{SiO2}} = 1.45$ and $n_{\mathrm{Al2O3}} = 1.74$, and the dispersive permittivity of the silver is calculated according to a Drude model which is fitted with the experimental data ($\varepsilon_{\mathrm{Ag}} = -87 - 8.7\mathrm{i}$ at the telecommunication wavelength $\lambda = 1550$ nm) [25].

For the proposed HP waveguides, there are two types of modes existing: TE modes which are dielectric-like modes and TM modes which are plasmonic-like modes. To obtain

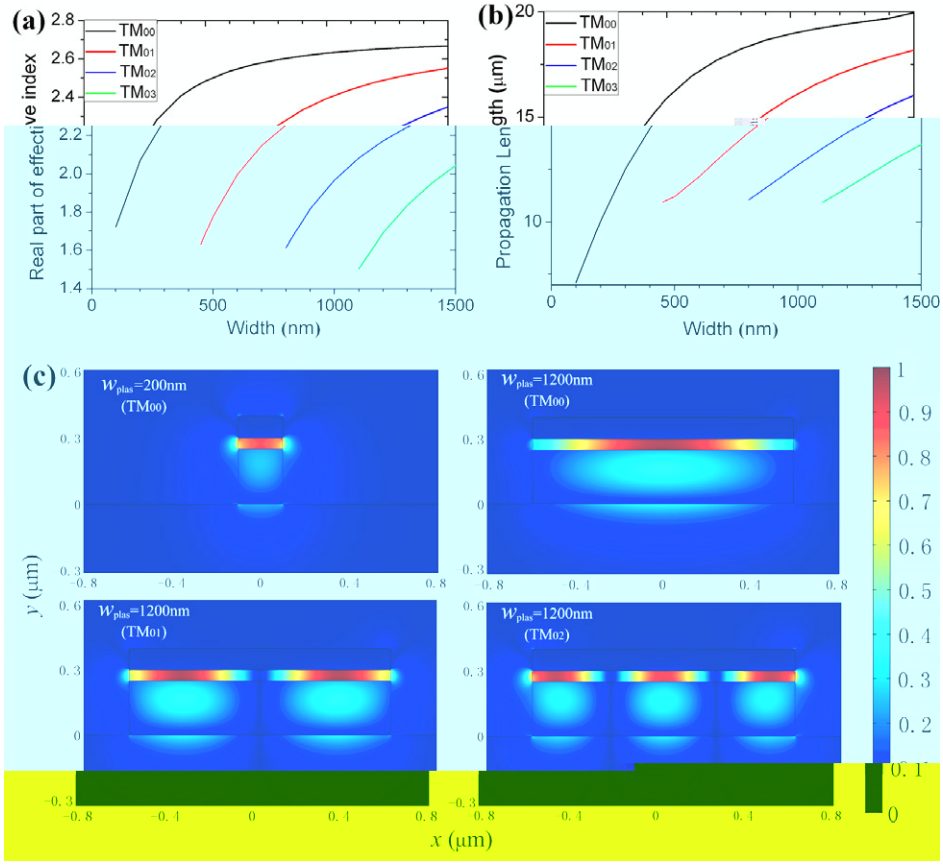

Figure 2. (a) The dependence of the real part of the effective index for $TM_{00} \sim TM_{03}$ modes on the width of the HP waveguide with $h_{Si} = 250$ nm, $h_{Al2O3} = 50$ nm and $h_{Ag} = 100$ nm, calculated by FEM. (b) The dependence of the propagation length for $TM_{00} \sim TM_{03}$ modes on the width of the HP waveguide. (c) The cross section of the electric field $|E_y|$ for the TM_{00} mode of a 200 nm wide HP waveguide and the TM_{00}, TM_{01} and TM_{02} modes for a 1200 nm wide HP waveguide.

the subwavelength mode confinement, we naturally focus on the TM modes. The dependences of the effective indices and propagation lengths for all supported TM modes on the widths of HP waveguides are plotted in figures 2(a) and (b), at $\lambda = 1550$ nm. The fundamental TM mode (TM_{00}) always exists for any width, and high-order modes emerge as the width increases. The cutoff widths for TM_{01}, TM_{02} and TM_{03} modes are about 450, 750 and 1100 nm. Accordingly, the widths of the HP MMI regime for the proposed 1×2 and 1×3 HP MMI power splitters should be larger than 750 and 1100 nm, respectively, in order to realize high resolution. To observe the modes more clearly, the normalized $|E_y|$ field distributions for the TM modes supported by a 200 nm wide and 1200 nm wide HP waveguide are shown in figure 2(c). For all these modes, the field distributions are similar and the electromagnetic energy is well confined in a subwavelength scale in the alumina layer.

For the 1×3 SOI-HP MMI power splitter, the width of the MMI regime is set to be $w_{MMI} = 1200$ nm. From the self-image principle, it is expected that the onefold, twofold and threefold images occur at the distances $L_1 = 3360$ nm, $L_2 = 1680$ nm and $L_3 = 1120$ nm, respectively. To confirm and optimize the power splitting, a home-made three-dimensional finite-difference time-domain (FDTD) code is used to simulate the wave propagation in the system. The parameters of the structure are the same as those used in the FEM simulations and the TM mode of the input SOI waveguide is excited by a Gaussian source with a central wavelength $\lambda_0 = 1550$ nm. Figure 3(a) shows the field distribution of E_y in the center of the alumina layer for the designed 1×3 SOI-HP MMI power splitter for which the length of the MMI regime is $L_{MMI} = 1200$ nm and the separation between the adjacent output HP waveguides is $s = 400$ nm. From figure 3(a), we notice that the electric field in the central output waveguide decays quickly compared to the two side output waveguides. This is mainly caused by the strong crosstalk between the three output waveguides, which can be solved by increasing their separation s or add S-bends to the two side output waveguides. Here, for numerical simplicity, we set the power detectors in the output waveguides at only 50 nm from the end of the MMI regime, whereby the influence of the crosstalk can be neglected.

The total transmission efficiency η and the power splitting ratio γ among the output waveguides are two important parameters to characterize the performance of an MMI power splitter [19]. Here the transmission efficiency is defined as $\eta = P_{out}/P_{in}$, where P_{out} is the power in the output HP waveguide and P_{in} is the power in the input SOI waveguide; more specifically, γ is defined as the ratio between the power transmitted to the central output waveguide and the average

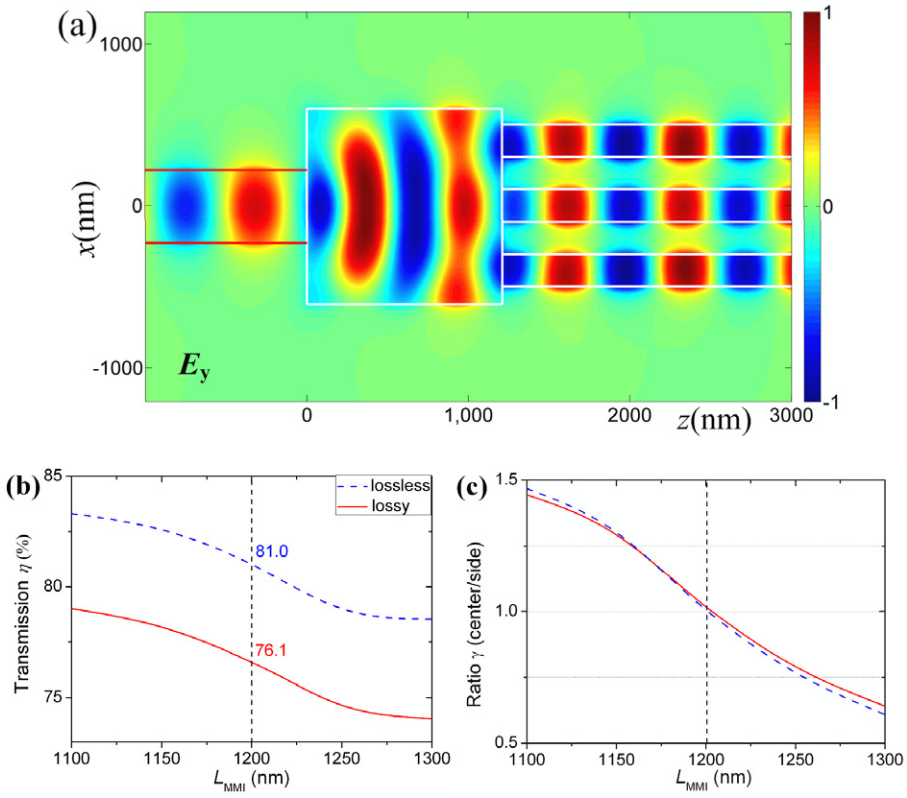

Figure 3. (a) The E_y field distribution in the center plane of the alumina layer for a 1×3 SOI-HP MMI power splitter, calculated by FDTD. (b) The dependence of total transmission η on the length of the MMI regime L_{MMI} (red solid line), compared with the same design but with lossless silver (blue dashed line). (c) The dependence of splitting ratio γ on the length of the MMI regime L_{MMI} (red solid line), compared with the same design but with lossless silver (blue dashed line).

power transmitted to the two side output waveguides [24]. The values of η and γ at different MMI lengths are plotted in figures 3(b) and (c), respectively. As shown in figure 3(c) (red solid line), the splitting ratio γ is very sensitive to the length of the MMI regime. As L_{MMI} increases from 1100 to 1300 nm, γ decreases from 1.45 to 0.64, which means more and more power is transmitted to the side waveguides. To realize a balanced power splitting (1:1:1), the length of the MMI regime should be $L_{MMI} = 1200$ nm, at which the total transmission is $\eta = 76.1\%$. There is a little difference between the numerical simulated and theoretical predicted values of L_{MMI} which is probably caused by the mode mismatch between the SOI waveguide and the HP waveguide. As a comparison, we also show the total transmission η and the splitting ratio γ for the same structure but with a lossless silver layer in figures 3(b) and (c) (blue dashed lines). In such a system, attenuation is solely due to the insertion loss [19]. The total transmission η of 81.0% is achieved at $L_{MMI} = 1200$ nm. The γ curve is almost the same as that for the lossy silver case, which means the propagation loss influences equally all the output waveguides. To further reduce the insertion loss, HP tapers can be adopted at the output interfacing of the MMI device [16, 17]. But it will nevertheless increase the propagation loss and in turn reduce the total transmission.

For a 1×2 SOI-HP MMI power splitter, we similarly set the width of the MMI regime at $w_{MMI} = 800$ nm for which the twofold image is expected to occur at the distance $L_2 = 847$ nm by equation (3). The corresponding field distribution of E_y and the dependence of the total transmission η on L_{MMI} are plotted in figure 4. At $L_{MMI} = 820$ nm, the highest total transmission is achieved with $\eta = 78.3\%$ (figure 4(b), red solid line) which again is higher than the designs with HP tapers. With a lossless silver layer, the total transmission at $L_{MMI} = 820$ nm increases to 82.1%. There is also a little difference between the FDTD simulated and theoretical predicted values of L_{MMI}, which is similar to the 1×3 SOI-HP MMI power splitter.

According to equation (3), the position for the N-fold image is sensitive to the wavelength, and so is the performance of the whole device. To gain quantitative knowledge about the influence of the wavelength, we calculate the variations of the total transmission η and the splitting ratio γ in the wavelength range of 1500–1600 nm for the 1×2 ($w_{MMI} = 800$ nm, $L_{MMI} = 820$ nm) and the 1×3 ($w_{MMI} = 1200$ nm, $L_{MMI} = 1200$ nm) SOI-HP MMI power splitters. The results are plotted in figure 5. Notice that, for the 1×2 SOI-HP MMI power splitter, γ is always 1. From figure 5, for both splitters the total transmission decreases slowly but always remains higher than 70% as the wavelength increases from 1500 to 1600 nm. For the 1×3 HP MMI power splitter, the splitting ratio varies sharply. To limit the imbalance in power splitting to be smaller than 10%, i.e. $0.9 \leqslant \gamma \leqslant 1.1$, the wavelength should be in the range of 1543–1555 nm.

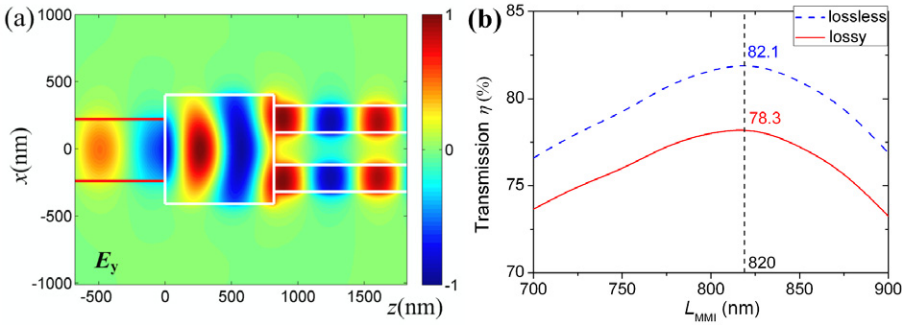

Figure 4. The E_y field distribution in the center plane of the alumina layer for a 1 × 2 SOI-HP MMI power splitter, calculated by FDTD. (b) The dependence of total transmission η on the length of the MMI regime L_{MMI} (red solid line), compared with the same design but with lossless silver (blue dashed line).

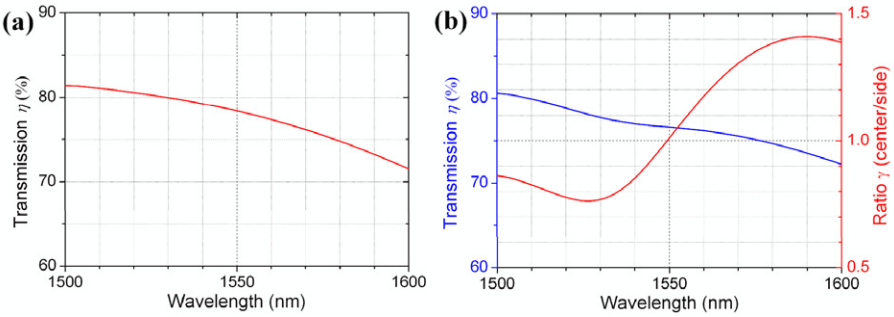

Figure 5. The total transmission η in the wavelength range 1500–1600 nm for a 1 × 2 SOI-HP MMI power splitter with w_{MMI} = 800 nm and L_{MMI} = 820 nm, calculated by FDTD. (b) The total transmission η and the splitting ratio γ in the wavelength range 1500–1600 nm for a 1 × 3 SOI-HP MMI power splitter with w_{MMI} = 1200 nm and L_{MMI} = 1200 nm.

4. Effect of possible misalignment in fabrication

In section 3, we have theoretically studied the performance of SOI-HP MMI power splitters and obtained the optimized parameters for the 1 × 3 and 1 × 2 configurations. However, it is unavoidable that some errors during fabrication would occur which may lead to deviations from the original design. As shown in figure 1(a), the input and output waveguides are placed in positions symmetric to the yz plane to realize a balanced splitting. If there exists some misalignment of the input and output waveguides from their designed positions during the fabrication procedure, the balanced power splitting will be broken. If a lateral shift only occurs for the input waveguide, the imbalance of the power splitting is mainly caused by the appearance of odd modes according to equation (2). If such a dislocation occurs only for the output waveguides, the imbalance is mainly caused by the mode mismatch. In an actual fabrication, the amount of misalignment is limited by the resolution limit of the fabrication procedure, which, e.g. for the electron-beam lithography and lift-off procedure, is smaller than 50 nm.

Figure 6(a) shows the dependences of the transmission on the lateral shifts of the waveguides for a 1 × 3 SOI-HP MMI power splitter (w_{MMI} = 1200 nm, L_{MMI} = 1200 nm). The total transmission and the transmission to the center output waveguide are almost unchanged, regardless of whether the shift happens for the input waveguide or the output waveguides; however, the transmission to the side output waveguides will be subject to a linear increase or decrease with respect to the shift. As the shift increases from 0 to 50 nm, the transmissions of three output waveguides change from a balanced splitting of 25.4%:25.3%:25.4% (in total 76.1%) to 28.8%:25.6%:21.7% (in total 76.1%) in the case that the shift is for the input waveguide, compared to 29.5%:25.3%:20.7% (in total 75.5%) in the case that the shift is for the output waveguides. Therefore in terms of total transmission, the influence of a shift due to misalignment is not significant, while a misalignment does adversely affect a balanced splitting.

The dependences of the transmission on the waveguide shifts for a 1×2 SOI-HP MMI power splitter (w_{MMI} = 800 nm, L_{MMI} = 820 nm) is plotted in figure 6(b). As the shift increases from 0 to 50 nm, the transmissions of three output waveguides change from a balanced splitting of 39.2%:39.2% (in total 78.3%) to 44.5%:33.8% (in total 78.3%) in the case that the shift occurs for the input waveguide, compared to 40.2%:36.7% (in total 76.9%) in the case that the shift occurs for the output waveguides. Here it is noticed that the influence of a shift on the input waveguide is more severe than that on the output waveguides. One should therefore pay more attention in the fabrication procedure to reduce the shift of the input waveguide in order to realize a balanced power splitting.

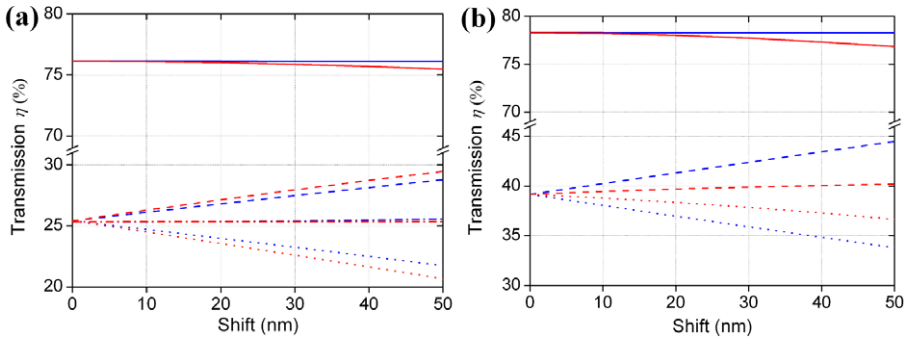

Figure 6. The dependences of the transmissions on the shifts of the access waveguides in the x direction, calculated by FDTD. (a) The total transmission (solid line) and the transmissions of the top (dashed line), center (dashed–dotted line) and bottom (dotted line) output waveguides for a 1×3 SOI-HP MMI power splitter ($w_{\mathrm{MMI}} = 1200$ nm, $L_{\mathrm{MMI}} = 1200$ nm) with the shift of the input (blue line) and output (red line) waveguides. (b) The total transmission (solid line) and the transmissions of the top (dashed line) and bottom (dotted line) output waveguides for a 1×2 SOI-HP MMI power splitter ($w_{\mathrm{MMI}} = 800$ nm, $L_{\mathrm{MMI}} = 820$ nm) with the shift of the input (blue line) and output (red line) waveguides.

5. Conclusions

In conclusion, we have proposed and theoretically studied the performance of $1 \times N$ SOI-HP MMI power splitters. The HP MMIs are implemented as a coupler between a standard SOI waveguide and several HP waveguides. With optimized structure parameters, the corresponding 1×3 and 1×2 SOI-HP MMI power splitters can realize balanced power splitting with the total transmission of 76.1% and 78.3%. The wavelength dependences of such SOI-HP couplers are also investigated. In particular, broadband splitting can be achieved with the 1×2 SOI-HP MMI splitter. Furthermore, the effect of possible misalignment of the input and output waveguides on both the total transmission and the balance of power splitting is discussed. We expect that the proposed $1 \times N$ SOI-HP MMI can serve an important role in near-future nanophotonic systems that incorporate both silicon photonics and plasmonics.

Acknowledgments

This work is supported by the Swedish Foundation for Strategic Research (SSF) and the Swedish Research Council (VR).

References

[1] Maier S A, Barclay P E, Johnson T J, Friedman M D and Painter O 2004 Low-loss fiber accessible plasmon waveguide for planar energy guiding and sensing *Appl. Phys. Lett.* **84** 3990

[2] Maier S A, Kik P G, Atwater H A, Meltzer S, Harel E, Koel B E and Requicha A A G 2003 Local detection of electromagnetic energy transport below the diffraction limit in metal nanoparticle plasmon waveguides *Nat. Mater.* **2** 229–32

[3] Charbonneau R, Lahoud N, Mattiussi G and Berini P 2005 Demonstration of integrated elements based on long-ranging surface plasmon polaritons *Opt. Express* **13** 977–84

[4] Takahara J, Yamagishi S, Taki H, Morioto A and Kabayashi T 1997 Guiding of a one-dimensional optical beam with nanometer diameter *Opt. Lett.* **22** 475–7

[5] Degiron A, Cho S Y, Tyler T, Jokerst N M and Smith D R 2009 Directional coupling between dielectric and long-range plasmon waveguides *New J. Phys.* **11** 015002

[6] Bozhevolnyi S I, Volkov V S, Devaux E, Laluet J Y and Ebbesen T W 2006 Channel plasmon subwavelength waveguide components including interferometers and ring resonators *Nature* **440** 508–11

[7] Pile D F P, Ogawa T, Gramotnev D K, Okamoto T, Haraguchi M, Fukui M and Matsuo S 2005 Theoretical and experimental investigation of strongly localized plasmons on triangular metal wedges for subwavelength waveguiding *Appl. Phys. Lett.* **87** 061106

[8] Yan M and Qiu M 2007 Guided plasmon polariton at 2D metal corners *J. Opt. Soc. Am.* B **24** 2333–42

[9] Chen L, Shakya J and Lipson M 2006 Subwavelength confinement in integrated metal slot waveguide on silicon *Opt. Lett.* **31** 2133–5

[10] Delacour C, Blaize S, Grosse P, Fedeli J M, Bruyant A, Salas-Montiel R, Lerondel G and Chelnoko A 2010 Efficient directional coupling between silicon and copper plasmonic nanoslot waveguides: toward metal–oxide–silicon nanophotonics *Nano Lett.* **10** 2922–6

[11] Alam M Z, Meier J, Aitchison J S and Mojahedi M 2010 Propagation characteristics of hybrid modes supported by metal-low-high index waveguides and bends *Opt. Express* **18** 12971–9

[12] Oulton R F, Sorger V J, Genov D A, Pile D F P and Zhang X 2008 A hybrid plasmonic waveguide for subwavelength confinement and long-range propagation *Nat. Photon.* **2** 496–500

[13] Oulton R F, Bartal G, Pile D F P and Zhang X 2008 Confinement and propagation characteristics of subwavelength plasmonic modes *New J. Phys.* **10** 105018

[14] Slavador R, Martinez A, Meca C G, Ortuno R and Marti J 2008 Analysis of hybrid dielectric plasmonic waveguides *IEEE J. Quantum Electron.* **14** 1496–501

[15] Dai D and He S 2009 A silicon-based hybrid plasmonic waveguide with a metal cap for a nano-scale light confinement *Opt. Express* **17** 16646–53

[16] Song Y, Wang J, Li Q, Yan M and Qiu M 2010 Broadband coupler between silicon waveguide and hybrid plasmonic waveguide *Opt. Express* **18** 13173–9

[17] Wu M, Han Z and Van V 2010 Conductor-gap-silicon plasmonic waveguides and passive components at subwavelength scale *Opt. Express* **18** 11728–36

[18] Wang J, Guan X, He Y, Shi Y, Wang Z, He S, Holmström P, Wosinski L, Thylen L and Dai D 2011 Sub-μm^2 power splitters by using silicon hybrid plasmonic waveguides *Opt. Express* **19** 838–47

[19] Soldano L B and Pennings E C M 1995 Optical multimode interference devices based on self-imaging-principles and applications *J. Lightwave Technol.* **13** 615–27

[20] Bachmann M, Besse P A and Melchior H 1994 General self-imaging properties in $N \times N$ multimode interference couplers including phase relations *Appl. Opt.* **33** 3905–11

[21] Ulrich R and Kamiya T 1978 Resolution of self-images in planar optical waveguides *J. Opt. Soc. Am.* **68** 583–92

[22] Han Z and He S 2007 Multimode interference effect in plasmonic subwavelength waveguides and an ultra-compact power splitter *Opt. Commun.* **278** 199–203

[23] Yuan G H, Wang P, Lu Y H and Ming H 2009 Multimode interference splitter based on dielectric-loaded surface plasmon polariton waveguides *Opt. Express* **17** 12594–600

[24] Tsai Y J, Degiron A, Jokerst N M and Smith D R 2009 Plasmonic multi-mode interference couplers *Opt. Express* **17** 17471–82

[25] Palik E D 1998 *Handbook of Optical Constants of Solids* (New York: Academic)